Spin-state Switching of Spin-Crossover Complexes on Cu(111) Evidenced by Spin-Flip Spectroscopy

Sven Johannsen, Alexander Weismann, Karl Ridier, Richard Berndt, Manuel Gruber

▶ **To cite this version:**

Sven Johannsen, Alexander Weismann, Karl Ridier, Richard Berndt, Manuel Gruber. Spin-state Switching of Spin-Crossover Complexes on Cu(111) Evidenced by Spin-Flip Spectroscopy. 2023. hal-04316911

HAL Id: hal-04316911
https://hal.science/hal-04316911

Preprint submitted on 30 Nov 2023

HAL is a multi-disciplinary open access archive for the deposit and dissemination of scientific research documents, whether they are published or not. The documents may come from teaching and research institutions in France or abroad, or from public or private research centers.

L'archive ouverte pluridisciplinaire **HAL**, est destinée au dépôt et à la diffusion de documents scientifiques de niveau recherche, publiés ou non, émanant des établissements d'enseignement et de recherche français ou étrangers, des laboratoires publics ou privés.

Copyright

Spin-state Switching of Spin-Crossover Complexes on Cu(111) Evidenced by Spin-Flip Spectroscopy

Sven Johannsen,[†] Alexander Weismann,[†] Karl Ridier,[‡] Richard Berndt,[†] and Manuel Gruber*,[¶]

†*Institut für Experimentelle und Angewandte Physik, Christian-Albrechts-Universität zu Kiel, 24098 Kiel, Germany*

‡*LCC, CNRS and Université de Toulouse, UPS, INP, 31077 Toulouse, France*

¶*Faculty of Physics and CENIDE, University of Duisburg-Essen, 47057 Duisburg, Germany*

E-mail: manuel.gruber@uni-due.de

Abstract

Spin-crossover compounds can be switched between two stable states with different magnetic moments, conformations, electronic, and optical properties, which opens appealing perspectives for technological applications including miniaturization down to the scale of single molecules. Although control of the spin states is crucial their direct identification is challenging in single-molecule experiments. Here we investigate the spin-crossover complex [Fe(HB(1,2,4-triazol-1-yl)$_3$)$_2$] on a Cu(111) surface with scanning tunneling microscopy. Spin crossover of single molecules in dense islands is achieved via electron injection. Spin-flip excitations are resolved in scanning tunneling spectra in a magnetic field enabling the direct identification of the spin state ($S = 2$) and the transitions ($m_s = -1 \rightarrow -2$ and $0 \rightarrow 1$) involved.

Spin-crossover (SCO) compounds are transition-metal complexes that can be switched between a low-spin (LS) and a high-spin (HS) state using various external stimuli such as temperature, light, and electrical current.[1] The spin-state transition is associated with a change of the molecular conformation and of the electronic and optical properties making such systems attractive for applications such in data storage, displays, and sensors,[2] possibly on the scale of single molecules.[3,4] Along this line, ultrathin films of SCO compounds have been fabricated by thermal evaporation under vacuum[5] and investigated.[4–23] Examples of successful electron and light induced excited spin state trapping (ELIESST, LIESST) have been reported from transport measurements[24–34] and scanning tunneling microscopy (STM).[20,23,35–44,44–47]

SCO complexes in direct contact with surfaces have attracted much interest but direct proof of single molecule SCO is difficult to obtain. The absence of switching of analogue Ni or Zn complexes,[45,46] where no SCO is expected, has provided indirect evidence in the case of Fe compounds. Comparisons with the results of density functional theory calculations, which predict different geometries and frontier orbital energies for the high and low spin states have also been used.[10,45,46] Finally, the observation of a Kondo resonance, which signals the presence of a localized spin, has been employed.[23,35,36] In the case of Fe(II) complexes only the HS state carries a magnetic moment and can lead to this effect. However, the Kondo effect is only observed when the coupling of the molecular spin and the conduction electrons happens to be suitably strong. A spin-state readout that is directly related to the magnetic moment of the metal-ion remains desirable.

Here we investigate the SCO complex [Fe(HB(1,2,4-triazol-1-yl)$_3$)$_2$] on a Cu(111) surface with STM. Individual molecules in large monolayer islands are switched by injecting electrons. Tunneling spectra of the molecule

in the HS state exhibit steps that shift in a magnetic field. These inelastic features reflect spin-flip excitations that represent direct information on the molecular spin state.

Results and Discussion

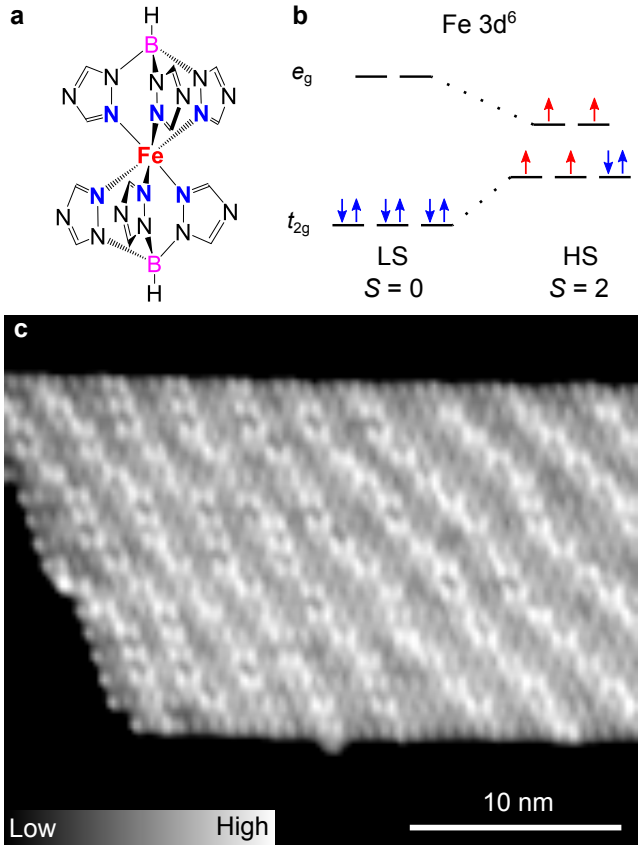

Figure 1: **a** Molecular structure of the complex [Fe(HB(1,2,4-triazol-1-yl)$_3$)$_2$]. **b** Schematic representation of the 3d orbitals for an Fe(II) ($3d^6$) complex in an octahedral ligand field. Blue (red) arrows indicate the orbital occupations with paired (unpaired) spins for low-spin (LS) and high-spin (HS) states. **c** Overview STM topograph (0.2 V, 5 pA, 30 × 25 nm^2) of a [Fe(HB(1,2,4-triazol-1-yl)$_3$)$_2$] island on Cu(111). The apparent height of the layer with respect to the Cu substrate is 220 pm. In addition to the molecular contrast, bright stripes with an apparent height of ≈ 30 pm are observed.

Self-Assembly on Cu(111)

The investigated [Fe(HB(1,2,4-triazol-1-yl)$_3$)$_2$] complex (Figure 1a) composed of two identical tridentate ligands, exhibits a transition temperature of ≈ 334 K in the bulk material.[48] As common for Fe(II) complexes in an octahedral ligand-field geometry, the electronic configuration in the LS and HS state leads to a total spin of $S = 0$ and $S = 2$, respectively (Figure 1b). Thin films (20 – 200 nm) of this compound prepared via sublimation in vacuum are of high quality, crystallize upon exposure to water vapor, and essentially exhibit the same transition temperature as bulk samples.[49]

Upon sublimation of submonolayer amounts of [Fe(HB(1,2,4-triazol-1-yl)$_3$)$_2$] on Cu(111), the molecules self-assemble into large islands, typically ≈ 20 nm wide and ≈ 40 – 80 nm long with an apparent height of ≈ 220 pm at 0.2 V (Figure 1c). The islands exhibit bright stripes with a periodicity of ≈ 3 nm. It seems that the molecules have an epitaxial relation with the substrate, as observed for the complex [Fe((3,5-(CH$_3$)$_2$Pz)$_3$BH)$_2$] on Au(111).[18] The stripes are likely due to misfit dislocations to release the strain within the layer caused by lattice mismatch.

Figure 2a shows a smaller area of the molecular layer on Cu(111). A regular arrangement of circular protrusions is observed along with fuzzy areas parallel to the top-left to bottom-right diagonal of the image. The protrusions and fuzzy areas correspond to individual molecules and the stripes, respectively (discussed above). To gain more information about the orientation of the molecules, we picked up a molecule from the layer by approaching the tip toward a protrusion and increasing the setpoint current from 5 to 20 pA at $V = 50$ mV. After depositing the molecule elsewhere, the remaining hole is observed as an horizontal depression (Figure 2b). Assuming that the image contrast is mainly caused by the upper part of a flat-lying molecule, we suggest that the orientation of the molecules is as shown in Figure 2c, where the lateral dimensions of the depression match with the upper two triazole groups of a molecule. Picking up further molecules from the same island leads to depressions with the same orientation (SI, Section 1), indicating that all molecules within an island have the same orientation. We therefore propose the molecular structure shown in Figure 2d and in the overlay of Figure 2a.

According to the proposed structure, the molecules form lines along the long direction of the islands with a periodicity of 1.1 nm (Figure 2d)). Within each line, two neighboring molecules are connected via C-H...N bonds between the underlying triazole groups (dotted lines in Figure 2d) leading to a center-to-center distance of ≈ 0.8 nm. Adjacent lines are vertically shifted and most probably stabilized by two C-H...N interactions between the upper triazole groups (dashed lines in Figure 2d). We note that the adsorbed molecule is chiral and the two enantiomers form different stackings leading to two types of islands (SI, Section 2 and 3).

Voltage Dependent Image Contrast

The appearance of the molecules as circular protrusions at 1.6 V (Figures 3a,c) presented above, drastically changes when the sample voltage is reduced to 0.2 V (Figures 3b,d). At this voltage, the molecules essentially appear as depressions (see Figure 3b, where green dots indicate the positions of the Fe atoms). The change of the sample voltage leads to a reduction of the apparent

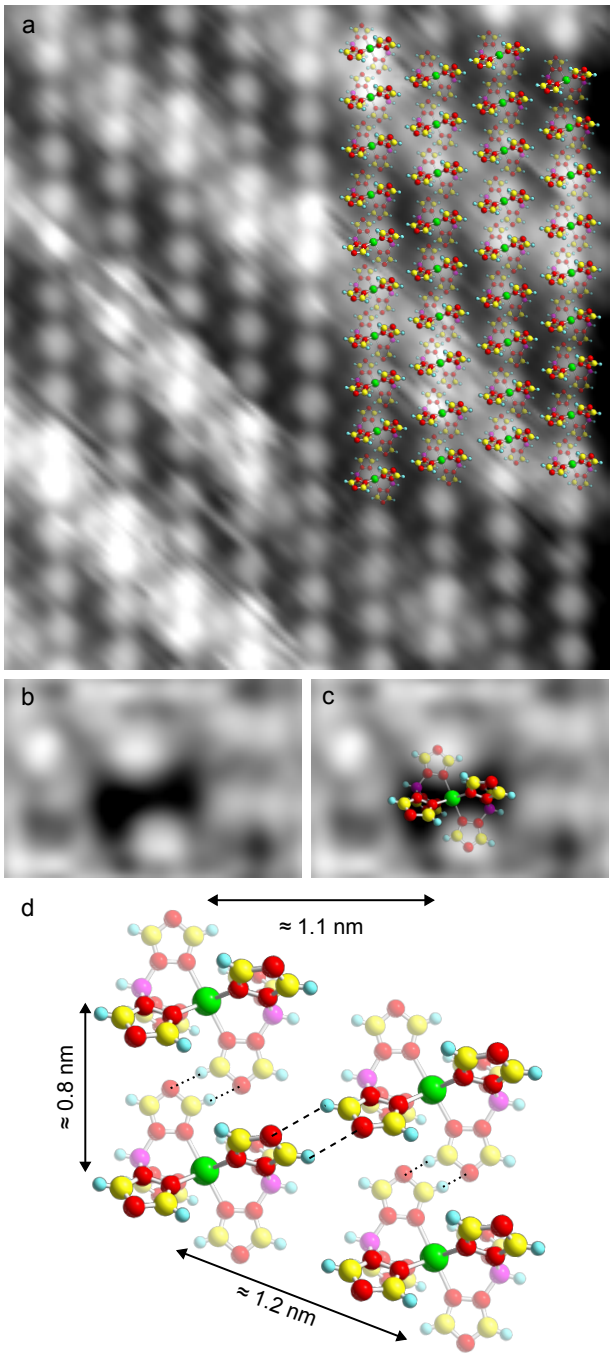

Figure 2: **a** STM topograph of [Fe(HB(1,2,4-triazol-1-yl)$_3$)$_2$] on Cu(111) with overlaid molecular models (1.6 V, 5 pA, 10×11 nm^2). **b** and **c** Zoomed STM topographs of an area from which a molecule has been picked up (200 mV, 5 pA, 3×2 nm^2). The remaining depression is horizontally elongated with a lateral extent matching that of the upper two triazole groups of a flat lying molecule. **d** Proposed arrangement of the molecules on the Cu(111) surface. For **a**–**d**, the transparency of the atoms indicates the height relative to the Cu(111) surface with transparent atoms being closer to the substrate. Green, yellow, red, purple, and cyan spheres respectively represent Fe, C, N, B, and H atoms.

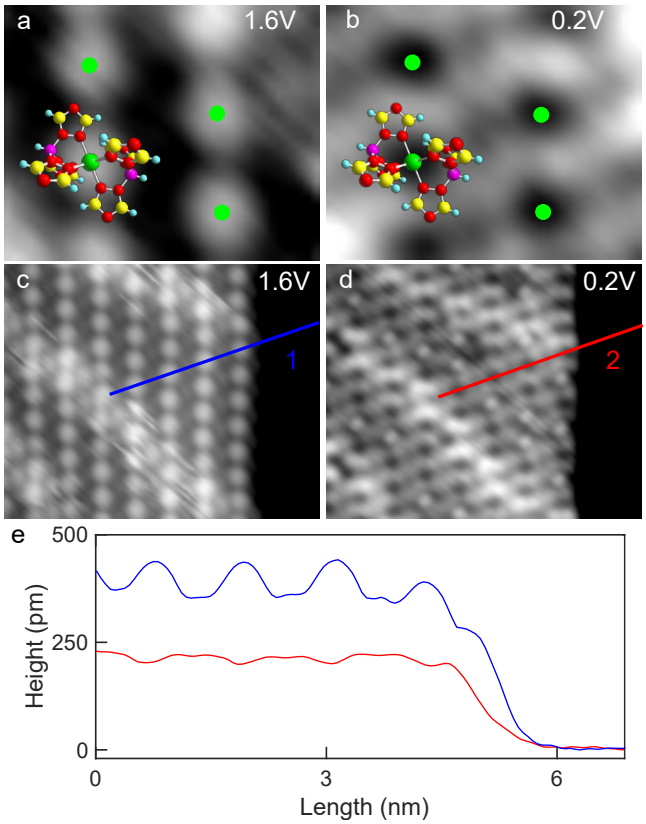

Figure 3: **a, b** Topographs of a 2.6×2.1 nm^2 area from a molecular island recorded at 1.6 and 0.2 V, respectively with $I = 5$ pA. While each [Fe(HB(1,2,4-triazol-1-yl)$_3$)$_2$] complex is imaged as a single protrusion at 1.6 V, the image contrast is reversed at 0.2 V. The suggested adsorption geometry is indicated by a superposed model and by green dots at the positions of the Fe ion centers. **c, d** Larger topographs (10×8 nm^2) of an island measured with the parameters used in panels **a** and **b**. At 1.6 V parallel columns of virtually identical protrusions are observed along with diagonal stripes. At 0.2 V the former protrusions, which correspond to single molecules, appear mostly as depressions (or as small protrusions upon switching as detailed below). **e** Cross-sectional profiles along the paths indicated by blue and red lines in **c** and **d**. At 1.6 V, the molecules appear approximately twice as high compared to 0.2 V (≈ 430 vs. ≈ 220 pm). The plateau at the right side of the height profiles shows the bare Cu(111) substrate.

height by almost a factor 2, from ≈ 430 pm at 1.6 V to ≈ 220 pm at 0.2 V (Figure 3e). This drastic modification of the molecular contrast indicates a large non-geometric contribution to the STM image. The importance of electronic contributions is further evidenced in images of island edges, where the border molecules appear smaller (SI, Section 4). One or more unoccupied molecular orbitals are expected to have energies between 0.2 and 1.6 eV. Unfortunately, the acquisition of $\mathrm{d}I/\mathrm{d}V$ spectra to confirm the presence of the orbitals failed because of large current fluctuations at voltages exceeding ≈ 0.5 V, as further discussed below. It is worth mentioning that, at a given voltage, all the molecules have the same appearance suggesting that they are all in the same pristine state.

Electron-Induced Switching

Switching of the molecules may be induced by injecting electrons at a sample voltage of ≈ 0.5 V or higher. Figure 4 shows an example. The pristine molecule appears as a depression at 0.2 V as previously described (white arrow in Figure 4a). After having placed the tip above the center of the depression, raising the voltage to 0.5 V for a few seconds, and decreasing it back to 0.2 V, while maintaining the current feedback loop active, the same molecule appears as a small protrusion (Figure 4b). The molecule may then be switched back to its pristine state using the same procedure (Figure 4c). Alternatively, for voltages above 0.5 V, telegraph noise is observed in time series of the tunneling current (feedback loop inactive). The low and high current levels correspond to a molecule appearing as a depression and protrusion, respectively.

Telegraph noise of the tunneling current was acquired for different tip-molecule distances and voltages, from which we can extract the switching rates (see Ref. 46 for details). The switching rates from a low (L) to a high (H) current value and vice versa evolve linearly with the tunneling current (Figure 5a) indicating that each switching event is caused by a single electron (the rate of a multi-electron process would evolve with I^N with $N > 1$). The probability of a tunneling electron to induce the switching is on the order of 10^{-7}, comparable to the highest reported yields for SCO molecules on surfaces (up to ≈ 8×10^{-7} in Ref. 46). The yield evolves rapidly with the applied voltage (Figure 5b). At 0.45 V, two transitions were observed in a time windows of 50 s (for $I = 5$ pA), while at 0.5 V switching is monitored every few seconds for currents as low as 5 pA. This implies that only electrons with an energy $\gtrsim 0.5$ eV can switch the molecules. Interestingly, a similar threshold has been determined for the compound $[Fe((3,5\text{-}(CH_3)_2Pz)_3BH)_2]$ on Cu(111),[20] suggesting that the two compounds might share a common microscopic switching mechanism.

Besides the local, controlled conversion of individual molecules, switching may be remotely triggered at distances up to ≈ 20 nm (Figure 6). Pulses of 2 V were applied on the Cu(111) surface (red dot in Figure 6a), which lead to the switching of many molecules, some of them encircled in red in Figure 6b. Interestingly, molecules up to ≈ 20 nm away from the location of the pulses were switched as well. This fairly efficient and long range remote switching is most probably due to hot electrons that propagate along the Cu(111) surface.[50]

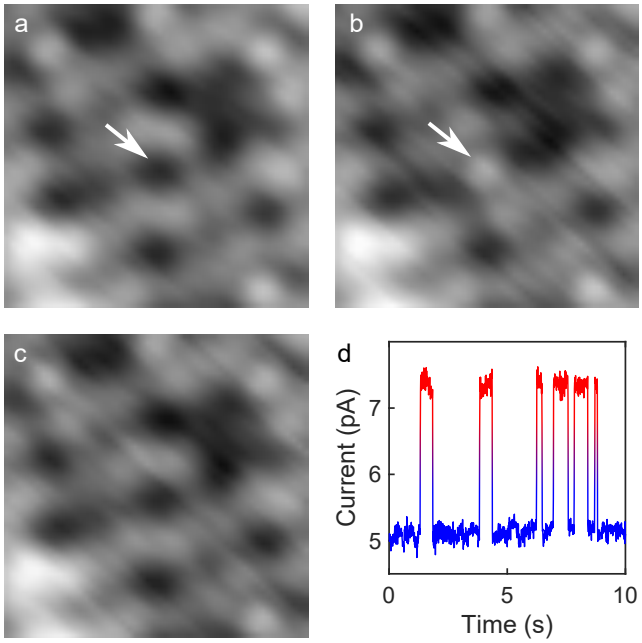

Figure 4: Reversible switching of an individual molecule under the tip. **a** Topograph (0.2 V, 5 pA, $3 \times 3\,\mathrm{nm}^2$) of an island with the molecule at the center (white arrow) in its pristine state appearing as a depression. **b** Same area imaged at 0.2 V after the voltage had been raised to 0.5 V for a few seconds with the tip placed above the central molecule (current feedback enabled). The former depression converted to a small protrusion. **c** After repeating the manipulation procedure, the center molecule reverted to its original state. **d** Time series of the tunneling current measured at $V = 0.5$ V with feedback disabled. Frequent switching is detected between current levels of ≈ 5.1 and 7.4 pA. Imaging at low bias revealed that the current levels reflect a depression and a protrusion, respectively.

Identification of Spin Transitions

High-resolution $\mathrm{d}I/\mathrm{d}V$ spectra of the molecules have been recorded with and without magnetic field. Molecules in the pristine (L) state essentially exhibit no features in the energy range ±8 meV (blue curve in Figure 7a). In contrast, the spectrum of the switched (H) state shows a pronounced dip centered at the Fermi level (red curve in Figure 7a). The dip is consistent with broadened inelastic excitation steps. The energy shift and amplitude decrease of these inelastic steps in a magnetic field of 8 T evidence that these excitations are related to the molecular spin. They are associated to spin flips involving an exchange of angular momentum between the molecule and the tunneling electrons.

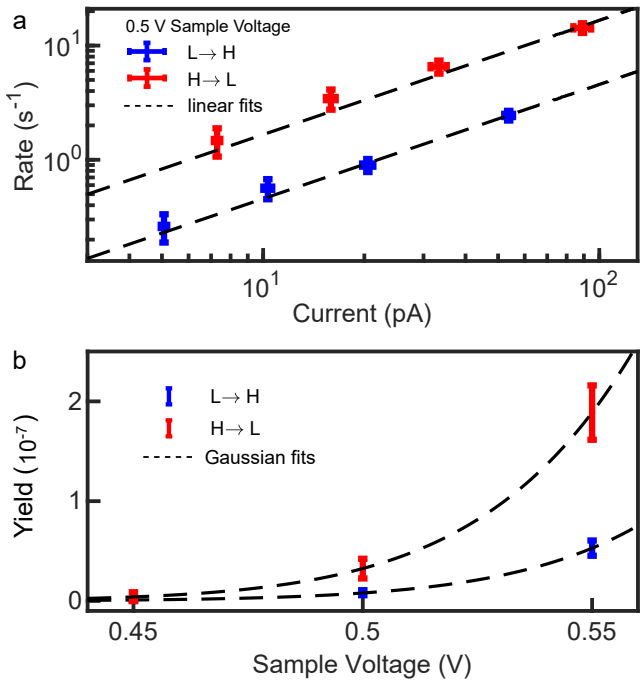

Figure 5: Switching rates and yields. **a** Rate of switching from the pristine L state to the H state and back as a function of the tunneling current. **b** Switching yields, defined as the switching rate normalized to the tunneling current, measured at three sample voltages. The uncertainty bars represent one standard deviation.

Based on these observations, we ascribe the pristine and switched states to the LS and HS states, respectively.

The presence of magnetic excitation steps at 0 T indicate that the molecular magnetic moment has a preferred orientation in the absence of magnetic field, *i. e.* magnetic anisotropy is present. We use the following phenomenological spin Hamiltonian to describe the energy of the magnetic states:[51]

$$\hat{H} = D\hat{S}_z^2 + E\left(\hat{S}_x^2 - \hat{S}_y^2\right) + g_z\mu_B B\hat{S}_z, \qquad (1)$$

where D and E are the uniaxial and transverse anisotropy parameters, $\hat{S} = \left(\hat{S}_x, \hat{S}_y, \hat{S}_z\right)$ the spin operator, g_z the Landé g-factor, μ_B the Bohr magneton, and B the applied magnetic field perpendicular to the surface. For simplicity, the quantization axis z is chosen perpendicular to the substrate. We consider a total spin $S = 2$, *i. e.* the formal spin of the HS state, which leads to an effective magnetic moment of $2 \cdot \sqrt{S\,(S+1)} \approx 4.9\,\mu_B$ per molecule comparable with that inferred from magnetometry measurements.[48] The diagonalization of the Hamiltonian of Eq. 1 leads to eigenstates $|\psi_i\rangle$ ($i = 1 \ldots 5$ for $S = 2$) and eigenenergies E_i, from which differential-conductance spectra are simulated.[52] The parameter set $D = 0.8\,\text{meV}$, $E \approx 0$, and $g_z = 1.8$ leads to the best agreement with the experimental data (dashed curves in Figure 7). (Fits considering $S = 1$ or 3 lead to much poorer agreements.) The uniaxial anisotropy parameter

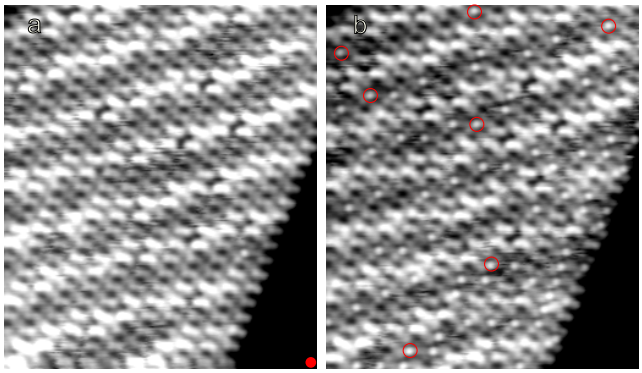

Figure 6: Long-range switching. **a** STM image of an island with molecules in the pristine (L) state. 10 pulses of 2 V for 200 ms each (I reaching ≈ 55 pA during the pulses) were applied on the Cu(111) substrate at the position indicated by a red dot. **b** STM image after the series of pulses. Several molecules switched to the H state, some of which are highlighted with red circles. Switched molecules are observed at distances as far as 21 nm away from the excitation point. This distance represents a lower bound as molecules outside the scanned area may have switched as well. Both images were acquired at 0.2 V, 5 pA ($15.6 \times 18.2\,\text{nm}^2$).

is very close to $D = 0.9\,\text{meV}$ as inferred from X-ray magnetic circular dichroism measurements of the complex $[\text{Fe}((3,5\text{-}(\text{CH}_3)_2\text{Pz})_3\text{BH})_2]$ on Cu(111), which lends further support to the model.

The fit of the $\text{d}I/\text{d}V$ spectra with the Hamiltonian of Equation 1 shows the consistency of the data with a spin $S = 2$. The exact values of the anisotropy parameters should be confirmed using more detailed measurements in magnetic vector fields or using complementary techniques. With $D = 0.8\,\text{meV}$, $E = 0$, $g = 1.8$ and in the absence of a magnetic field, the ground state of the system is $|\psi_1\rangle = |0\rangle$ (expressed in the basis $|S_z\rangle$), *i. e.* with a spin orientation in the plane of the molecular layer. The excitation steps then correspond to transitions to $|\psi_{2,3}\rangle = |\pm 1\rangle$ at $E_{2,3} = 0.8\,\text{meV}$, which are experimentally observed as a single transition (Figure 7b). In a magnetic field, the Zeeman term tends to favor large $|S_z|$ in contrast to the uniaxial anisotropy term ($D > 0$) that stabilizes small $|S_z|$. At 8 T, both terms are comparable in magnitude. As a consequence,$|0\rangle$ and $|-1\rangle$ are almost degenerate and so are $|+1\rangle$ and $|-2\rangle$ (Figure 7b). The separation of these two pairs is $\approx 1.6\,\text{meV}$. In other words, at 8 T, we essentially observe transitions from $|-1\rangle$ to $|-2\rangle$ and from $|0\rangle$ to $|1\rangle$.

It should be emphasized that the identification of the spin states via the observation of magnetic excitations in the $\text{d}I/\text{d}V$ spectra is not limited to SCO systems exhibiting magnetic anisotropy. In the case of an isotropic spin system, the Hamiltonian of Eq. 1 would be reduced to the Zeeman term, which splits the $|S_z\rangle$ states under a magnetic field. Transitions from $|-2\rangle$ to $|-1\rangle$ would then be observed at an energy $g\mu_B B$ ($\approx 0.9\,\text{meV}$ at 8 T

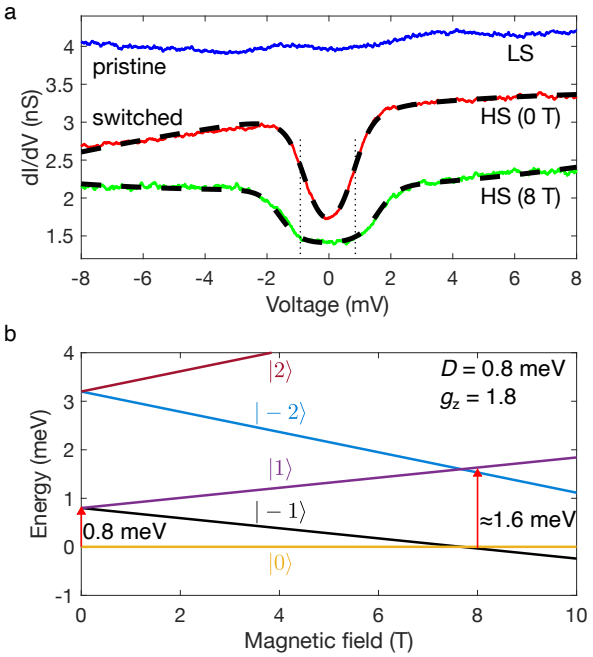

Figure 7: Identification of the spin states via spin-flip spectroscopy. **a** $\mathrm{d}I/\mathrm{d}V$ spectra acquired atop the center of a molecule in the pristine (blue, LS) and switched (red, HS) states at 1.7 K (with no external magnetic field). The spectrum of the switched molecule exhibits a dip consistent with broadened inelastic excitation steps (spin flips). In a magnetic field of 8 T, the steps are shifted to higher energies and have a lower amplitude (green), confirming the magnetic origin of the excitation steps. The spectra of the switched molecule can be conjointly fitted (dashed lines) using the spin Hamiltonian of Equation 1 with $S = 2$, $g = 1.8$, $D = 0.8$ meV and $E \approx 0$ (adjustable parameters) including temperature broadening ($T = 2.5$ K) as well as a cubic background. Spectra acquired over a pristine molecule under 8 T remain featureless (not shown). The vertical dotted lines are guide to the eye to better visualize the increase of the step energies with magnetic field. The LS and HS (8 T) spectra have been vertically shifted by +1 and −1 nS for clarity. Prior to the voltage sweep, the current feedback was opened at 10 mV and 30 pA. **b** Energies of the eigenstates $|S_z\rangle$ as a function of the external magnetic field for $D = 0.8$ meV, $E = 0$, and $g_z = 1.8$. The vertical red arrows indicate possible transitions at 0 and 8 T via spin-flip processes with tunnel electrons.

for $g = 2$) in $\mathrm{d}I/\mathrm{d}V$ spectra.

Conclusion

We investigated the molecular SCO complex $[\mathrm{Fe(HB(1,2,4\text{-}triazol\text{-}1\text{-}yl)_3)_2}]$ adsorbed on a Cu(111) surface with scanning tunneling microscopy. The complexes self-assemble into an ordered structure and form large islands. The molecules are efficiently switched between the LS and HS states by injecting electrons. This may be realized locally by placing the tip above a targeted molecule with a mild voltage ($\gtrsim 0.5$ V) or by injecting more energetic electrons ($V \approx 2$ V) into the substrate. The latter procedure allows the remote switching of molecules in a radius of at least 20 nm from the excitation point. Spectra acquired atop the center of HS molecules reveal excitation steps that change in an applied magnetic field, while no features are found for LS molecules. The inelastic steps correspond to magnetic excitations of the HS molecule and show that the magnetic moment of the molecule has a preferred orientation. Besides enabling an unambiguous identification of the spin states, these results suggest that manipulation of the quantum spins of the SCO complexes may be feasible.

Acknowledgement We acknowledge financial support from the European Union's Horizon 2020 program, grant number 766726. M.G. acknowledges funding from the Deutsche Forschungsgemeinschaft (DFG; Project-ID 278162697 - CRC 1242, Project A08). We are indebted to D. Moreno, D. Ecija and F. Calleja (IMDEA Nanoscience, Madrid, Spain) for their involvement in initial evaporation and room-temperature STM tests on this compound. We thank G. Molnar and A. Bousseksou (LCC-CNRS, Toulouse, France) for fruitful discussions.

Methods

Synthesis

The $[\mathrm{Fe(HB(1,2,4\text{-}triazol\text{-}1\text{-}yl)_3)_2}]$ powder was synthesized following the description of Ref. 48.

STM

The Cu(111) surface was prepared by cycles of Ar ion bombardment (1.5 keV) and annealing to 500 °C. $[\mathrm{Fe(HB(1,2,4\text{-}triazol\text{-}1\text{-}yl)_3)_2}]$ was sublimated from a heated crucible (≈ 210 °C). STM tips were electrochemically etched from W wire and annealed *in vacuo*. Experiments were carried out in ultrahigh vacuum mostly with a STM operated at ≈ 4.6 K (Createc). $\mathrm{d}I/\mathrm{d}V$ spectra were acquired at 1.7 K with a Unisoku USM1300 STM. The shown $\mathrm{d}I/\mathrm{d}V$ spectra are obtained from numerical derivation of the current, followed by a convolution with a Gaussian for low-pass filtering.

Author contributions

MG, RB, and KR designed the experiment. SJ, AW performed the STM experiments. SJ, MG, and RB analyzed the STM data. MG wrote the manuscript with contributions from all authors. All authors discussed the results and commented on the manuscript.

Data availability

Raw data may be obtained from the corresponding authors upon reasonable request.

Supporting Information

Supporting Information about molecule removal from an island, adsorption-induced chirality, chirality of islands, and reduced height of edge molecules

References

1. Gütlich, P.; Garcia, Y.; Goodwin, H. A. Spin Crossover Phenomena in Fe (II) Complexes. *Chem. Soc. Rev.* **2000**, *29*, 419–427.

2. Molnár, G.; Rat, S.; Salmon, L.; Nicolazzi, W.; Bousseksou, A. Spin Crossover Nanomaterials: From Fundamental Concepts to Devices. *Adv. Mater.* **2018**, *30*, 17003862.

3. Bellec, A.; Lagoute, J.; Repain, V. Molecular Electronics: Scanning Tunneling Microscopy and Single-Molecule Devices. *C R Chim* **2018**, *21*, 1287–1299.

4. Gruber, M.; Berndt, R. Spin-Crossover Complexes in Direct Contact with Surfaces. *Magnetochemistry* **2020**, *6*, 35.

5. Kumar, K. S.; Ruben, M. Sublimable Spin-Crossover Complexes: From Spin-State Switching to Molecular Devices. *Angew. Chem. Int. Ed.* **2021**, *60*, 7502–7521.

6. Bernien, M.; Wiedemann, D.; Hermanns, C. F.; Krüger, A.; Rolf, D.; Kroener, W.; Müller, P.; Grohmann, A.; Kuch, W. Spin Crossover in a Vacuum-Deposited Submonolayer of a Molecular Iron(II) Complex. *J. Phys. Chem. Lett.* **2012**, *3*, 3431–3434.

7. Palamarciuc, T.; Oberg, J. C.; El Hallak, F.; Hirjibehedin, C. F.; Serri, M.; Heutz, S.; Létard, J. F.; Rosa, P. Spin Crossover Materials Evaporated Under Clean High Vacuum and Ultra-High Vacuum Conditions: From Thin Films to Single Molecules. *J. Mater. Chem.* **2012**, *22*, 9690–9695.

8. Warner, B.; Oberg, J. C.; Gill, T. G.; El Hallak, F.; Hirjibehedin, C. F.; Serri, M.; Heutz, S.; Arrio, M.-A.; Sainctavit, P.; Mannini, M.; Poneti, G.; Sessoli, R.; Rosa, P. Temperature- And Light-Induced Spin Crossover Observed by X-Ray Spectroscopy on Isolated Fe(II) Complexes on Gold. *J. Phys. Chem. Lett.* **2013**, *4*, 1546–1552.

9. Bernien, M.; Naggert, H.; Arruda, L. M.; Kipgen, L.; Nickel, F.; Miguel, J.; Hermanns, C. F.; Krüger, A.; Krüger, D.; Schierle, E.; Weschke, E.; Tuczek, F.; Kuch, W. Highly Efficient Thermal and Light-Induced Spin-State Switching of an Fe(II) Complex in Direct Contact With a Solid Surface. *ACS Nano* **2015**, *9*, 8960–8966.

10. Bairagi, K.; Iasco, O.; Bellec, A.; Kartsev, A.; Li, D.; Lagoute, J.; Chacon, C.; Girard, Y.; Rousset, S.; Miserque, F.; Dappe, Y. J.; Smogunov, A.; Barreteau, C.; Boillot, M.-L.; Mallah, T.; Repain, V. Molecular-Scale Dynamics of Light-Induced Spin Cross-Over in a Two-Dimensional Layer. *Nat. Commun.* **2016**, *7*, 12212.

11. Kipgen, L.; Bernien, M.; Nickel, F.; Naggert, H.; Britton, A. J.; Arruda, L. M.; Schierle, E.; Weschke, E.; Tuczek, F.; Kuch, W. Soft-X-Ray-Induced Spin-state Switching of an Adsorbed Fe(II) Spin-crossover Complex. *J. Phys.: Condens. Matter* **2017**, *29*, 394003.

12. Zhang, X.; Costa, P. S.; Hooper, J.; Miller, D. P.; N'Diaye, A. T.; Beniwal, S.; Jiang, X.; Yin, Y.; Rosa, P.; Routaboul, L.; Gonidec, M.; Poggini, L.; Braunstein, P.; Doudin, B.; Xu, X.; Enders, A.; Zurek, E.; Dowben, P. A. Locking and Unlocking the Molecular Spin Crossover Transition. *Adv. Mater.* **2017**, *29*, 1702257.

13. Wäckerlin, C.; Donati, F.; Singha, A.; Baltic, R.; Decurtins, S.; Liu, S.-X.; Rusponi, S.; Dreiser, J. Excited Spin-State Trapping in Spin Crossover Complexes on Ferroelectric Substrates. *J. Phys. Chem. C* **2018**, *122*, 8202–8208.

14. Rohlf, S.; Gruber, M.; Flöser, B. M.; Grunwald, J.; Jarausch, S.; Diekmann, F.; Kalläne, M.; Jasper-Toennies, T.; Buchholz, A.; Plass, W.; Berndt, R.; Tuczek, F.; Rossnagel, K. Light-Induced Spin Crossover in an Fe(II) Low-Spin Complex Enabled by Surface Adsorption. *J. Phys. Chem. Lett.* **2018**, *9*, 1491–1496.

15. Kipgen, L.; Bernien, M.; Ossinger, S.; Nickel, F.; Britton, A. J.; Arruda, L. M.; Naggert, H.; Luo, C.; Lotze, C.; Ryll, H.; Radu, F.; Schierle, E.; Weschke, E.; Tuczek, F.; Kuch, W. Evolution of Cooperativity in the Spin Transition of an Iron(II) Complex on a Graphite Surface. *Nat. Commun.* **2018**, *9*, 2984.

16. Kumar, K. S.; Studniarek, M.; Heinrich, B.; Arabski, J.; Schmerber, G.; Bowen, M.; Boukari, S.; Beaurepaire, E.; Dreiser, J.; Ruben, M. Engineering On-Surface Spin Crossover: Spin-State Switching in a Self-Assembled Film of Vacuum-Sublimable Functional Molecule. *Adv. Mater.* **2018**, *30*, 1705416.

17. Rohlf, S.; Grunwald, J.; Jasper-Toennies, T.; Johannsen, S.; Diekmann, F.; Studniarek, M.; Berndt, R.; Tuczek, F.; Rossnagel, K.; Gruber, M. Influence of Substrate Electronic Properties on the Integrity and Functionality of an Adsorbed Fe(II) Spin-Crossover Compound. *J. Phys. Chem. C* **2019**, *123*, 17774.

18. Fourmental, C.; Mondal, S.; Banerjee, R.; Bellec, A.; Garreau, Y.; Coati, A.; Chacon, C.; Girard, Y.; Lagoute, J.; Rousset, S.; Boillot, M.-L.; Mallah, T.; Enachescu, C.; Barreteau, C.; Dappe, Y. J.; Smogunov, A.; Narasimhan, S.; Repain, V. Importance of Epitaxial Strain at a Spin-Crossover Molecule–Metal Interface. *J. Phys. Chem. Lett.* **2019**, *10*, 4103–4109.

19. Beniwal, S.; Sarkar, S.; Baier, F.; Weber, B.; Dowben, P. A.; Enders, A. Site Selective Adsorption of the Spin Crossover Complex $Fe(phen)_2(NCS)$ on Au(111). *J. Phys.: Condens. Matter* **2020**, *32*, 324003.

20. Tong, Y.; Kelai, M.; Bairagi, K.; Repain, V.; Lagoute, J.; Girard, Y.; Rousset, S.; Boillot, M.-L.; Mallah, T.; Enachescu, C.; Bellec, A. Voltage-Induced Bistability of Single Spin-Crossover Molecules in a Two-Dimensional Monolayer. *J. Phys. Chem. Lett.* **2021**, *12*, 11029–11034.

21. Rohlf, S.; Grunwald, J.; Kalläne, M.; Kähler, J.; Diekmann, F.; Ossinger, S.; Flöser, B.; Tuczek, F.; Rossnagel, K.; Gruber, M. Probing the Spin State of Spin-Crossover Complexes on Surfaces with Vacuum Ultraviolet Angle-Resolved Photoemission Spectroscopy. *J. Phys. Chem. C* **2021**, 14105–14116.

22. Kelai, M.; Repain, V.; Tauzin, A.; Li, W.; Girard, Y.; Lagoute, J.; Rousset, S.; Otero, E.; Sainctavit, P.; Arrio, M.-A.; Boillot, M.-L.; Mallah, T.; Enachescu, C.; Bellec, A. Thermal Bistability of an Ultrathin Film of Iron(II) Spin-Crossover Molecules Directly Adsorbed on a Metal Surface. *J. Phys. Chem. Lett.* **2021**, *12*, 6152–6158.

23. Gruber, M.; Miyamachi, T.; Davesne, V.; Bowen, M.; Boukari, S.; Wulfhekel, W.; Alouani, M.; Beaurepaire, E. Spin Crossover in $Fe(phen)_2(NCS)_2$ Complexes on Metallic Surfaces. *J. Chem. Phys.* **2017**, *146*, 092312.

24. Prins, F.; Monrabal-Capilla, M.; Osorio, E. A.; Coronado, E.; van der Zant, H. S. J. Room-Temperature Electrical Addressing of a Bistable Spin-Crossover Molecular System. *Adv. Mater.* **2011**, *23*, 1545–1549.

25. Osorio, E. A.; Ruben, M.; Seldenthuis, J. S.; Lehn, J. M.; van der Zant, H. S. J. Conductance Switching and Vibrational Fine Structure of a [2×2] Co_4^{II} Gridlike Single Molecule Measured in a Three-Terminal Device. *Small* **2010**, *6*, 174–178.

26. Harzmann, G. D.; Frisenda, R.; Zant, H. S. J. v. d.; Mayor, M. Single-Molecule Spin Switch Based on Voltage-Triggered Distortion of the Coordination Sphere. *Angew. Chem. Int. Ed.* **2015**, *54*, 13425–13430.

27. Frisenda, R.; Harzmann, G. D.; Celis Gil, J. A.; Thijssen, J. M.; Mayor, M.; van der Zant, H. S. J. Stretching-Induced Conductance Increase in a Spin-Crossover Molecule. *Nano Lett.* **2016**, *16*, 4733–4737.

28. Shalabaeva, V.; Ridier, K.; Rat, S.; Manrique-Juarez, M. D.; Salmon, L.; Séguy, I.; Rotaru, A.; Molnár, G.; Bousseksou, A. Room Temperature Current Modulation in Large Area Electronic Junctions of Spin Crossover Thin Films. *Appl. Phys. Lett.* **2018**, *112*, 013301.

29. Hao, G.; Mosey, A.; Jiang, X.; Yost, A. J.; Sapkota, K. R.; Wang, G. T.; Zhang, X.; Zhang, J.; N'Diaye, A. T.; Cheng, R.; Xu, X.; Dowben, P. A. Nonvolatile Voltage Controlled Molecular Spin State Switching. *Appl. Phys. Lett.* **2019**, *114*, 032901.

30. Zhang, Y.; Séguy, I.; Ridier, K.; Shalabaeva, V.; Piedrahita-Bello, M.; Rotaru, A.; Salmon, L.; Molnár, G.; Bousseksou, A. Resistance Switching in Large-Area Vertical Junctions of the Molecular Spin Crossover Complex $[Fe(HB(tz)_3)_2]$: ON/OFF Ratios and Device Stability. *J. Phys. Condens. Matter* **2020**, *32*, 214010.

31. Gee, A.; Jaafar, A. H.; Brachňaková, B.; Massey, J.; Marrows, C. H.; Šalitroš, I.; Kemp, N. T. Multilevel Resistance Switching and Enhanced Spin Transition Temperature in Single- and Double-Molecule Spin Crossover Nanogap Devices. *J. Phys. Chem. C* **2020**, *124*, 13393–13399.

32. Geest, E. P.; Shakouri, K.; Fu, W.; Robert, V.; Tudor, V.; Bonnet, S.; Schneider, G. F. Contactless Spin Switch Sensing by Chemo-Electric Gating of Graphene. *Adv. Mater.* **2020**, *32*, 1903575.

33. Konstantinov, N.; Tauzin, A.; Noumbé, U. N.; Dragoe, D.; Kundys, B.; Majjad, H.; Brosseau, A.; Lenertz, M.; Singh, A.; Berciaud, S.; Boillot, M.-L.; Doudin, B.; Mallah, T.; Dayen, J.-F. Electrical Read-Out of Light-Induced Spin Transition in Thin

Film Spin Crossover/Graphene Heterostructures. *J. Mater. Chem. C* **2021**, *9*, 2712–2720.

34. Stegmann, P.; Gee, A.; Kemp, N. T.; König, J. Statistical Analysis of Spin Switching in Coupled Spin-Crossover Molecules. *Phys. Rev. B* **2021**, *104*, 125431.

35. Gopakumar, T. G.; Matino, F.; Naggert, H.; Bannwarth, A.; Tuczek, F.; Berndt, R. Electron-Induced Spin Crossover of Single Molecules in a Bilayer on Gold. *Angew. Chem. Int. Ed.* **2012**, *51*, 6262–6266.

36. Miyamachi, T.; Gruber, M.; Davesne, V.; Bowen, M.; Boukari, S.; Joly, L.; Scheurer, F.; Rogez, G.; Yamada, T. K.; Ohresser, P.; Beaurepaire, E.; Wulfhekel, W. Robust Spin Crossover and Memristance Across a Single Molecule. *Nat. Commun.* **2012**, *3*, 938.

37. Gruber, M.; Davesne, V.; Bowen, M.; Boukari, S.; Beaurepaire, E.; Wulfhekel, W.; Miyamachi, T. Spin State of Spin-Crossover Complexes: From Single Molecules to Ultrathin Films. *Phys. Rev. B* **2014**, *89*, 195415.

38. Jasper-Tönnies, T.; Gruber, M.; Karan, S.; Jacob, H.; Tuczek, F.; Berndt, R. Deposition of a Cationic Fe^{III} Spin-Crossover Complex on Au(111): Impact of the Counter Ion. *J. Phys. Chem. Lett.* **2017**, *8*, 1569–1573.

39. Jasper-Toennies, T.; Gruber, M.; Karan, S.; Jacob, H.; Tuczek, F.; Berndt, R. Robust and Selective Switching of an Fe^{III} Spin-Crossover Compound on Cu_2N/Cu(100) with Memristance Behavior. *Nano Lett.* **2017**, *17*, 6613.

40. Atzori, M.; Poggini, L.; Squillantini, L.; Cortigiani, B.; Gonidec, M.; Bencok, P.; Sessoli, R.; Mannini, M. Thermal and Light-Induced Spin Transition in a Nanometric Film of a New High-Vacuum Processable Spin Crossover Complex. *J. Mater. Chem. C* **2018**, *6*, 8885–8889.

41. Köbke, A.; Gutzeit, F.; Röhricht, F.; Schlimm, A.; Grunwald, J.; Tuczek, F.; Studniarek, M.; Longo, D.; Choueikani, F.; Otero, E.; Ohresser, P.; Rohlf, S.; Johannsen, S.; Diekmann, F.; Rossnagel, K.; Weismann, A.; Jasper-Toennies, T.; Näther, C.; Herges, R.; Berndt, R. *et al.* Reversible Coordination-Induced Spin-State Switching in Complexes on Metal Surfaces. *Nat. Nanotechnol.* **2020**, *15*, 38.

42. Brandl, T.; Johannsen, S.; Häussinger, D.; Suryadevara, N.; Prescimone, A.; Bernhard, S.; Gruber, M.; Ruben, M.; Berndt, R.; Mayor, M. Iron in a Cage: Fixation of a Fe(II)tpy_2 Complex by Fourfold Interlinking. *Angew. Chem. Int. Ed.* **2020**, *59*, 15947.

43. Zhang, L.; Tong, Y.; Kelai, M.; Bellec, A.; Lagoute, J.; Chacon, C.; Girard, Y.; Rousset, S.; Boillot, M.; Rivière, E.; Mallah, T.; Otero, E.; Arrio, M.; Sainctavit, P.; Repain, V. Anomalous Light-Induced Spin-State Switching for Iron(II) Spin-Crossover Molecules in Direct Contact with Metal Surfaces. *Angew. Chem. Int. Ed.* **2020**, *59*, 13341–13346.

44. Johannsen, S.; Schüddekopf, S.; Ossinger, S.; Grunwald, J.; Tuczek, F.; Gruber, M.; Berndt, R. Three-State Switching of an Fe Spin Crossover Complex. *J. Phys. Chem. C* **2022**, *126*, 7238 – 7244.

45. Johannsen, S.; Gruber, M.; Barreteau, C.; Seredyuk, M.; Real, J. A.; Markussen, T.; Berndt, R. Spin-Crossover and Fragmentation of Fe(neoim)$_2$ on Ag and Au. *J. Phys. Chem. Lett.* **2023**, *14*, 7814–7823.

46. Johannsen, S.; Ossinger, S.; Markussen, T.; Tuczek, F.; Gruber, M.; Berndt, R. Electron-Induced Spin-Crossover in Self-Assembled Tetramers. *ACS Nano* **2021**, *15*, 11770–11778.

47. Johannsen, S.; Ossinger, S.; Grunwald, J.; Herman, A.; Wende, H.; Tuczek, F.; Gruber, M.; Berndt, R. Spin Crossover in a Co Complex on Ag(111). *Angew. Chem. Int. Ed.* **2022**, *61*, e202115892.

48. Rat, S.; Ridier, K.; Vendier, L.; Molnár, G.; Salmon, L.; Bousseksou, A. Solvatomorphism and Structural-Spin Crossover Property Relationship in bis[hydrotris(1,2,4-triazol-1-yl)borate]iron(II). *CrystEngComm* **2017**, *19*, 3271–3280.

49. Shalabaeva, V.; Rat, S.; Manrique-Juarez, M. D.; Bas, A.-C.; Vendier, L.; Salmon, L.; Molnár, G.; Bousseksou, A. Vacuum deposition of high-quality thin films displaying spin transition near room temperature. *J. Mater. Chem. C* **2017**, *5*, 4419–4425.

50. Leisegang, M.; Kügel, J.; Klein, L.; Bode, M. Analyzing the Wave Nature of Hot Electrons with a Molecular Nanoprobe. *Nano Lett.* **2018**, *18*, 2165–2171.

51. Hirjibehedin, C. F.; Lin, C.-Y.; Otte, A. F.; Ternes, M.; Lutz, C. P.; Jones, B. A.; Heinrich, A. J. Large Magnetic Anisotropy of a Single Atomic Spin Embedded in a Surface Molecular Network. *Science* **2007**, *317*, 1199–1203.

52. Ternes, M. Spin Excitations and Correlations in Scanning Tunneling Spectroscopy. *New Journal of Physics* **2015**, *17*, 063016.

Supporting Information: Spin-state Switching of Spin-Crossover Complexes on Cu(111) Evidenced by Spin-Flip Spectroscopy

Sven Johannsen,[†] Alexander Weismann,[†] Karl Ridier,[‡] Richard Berndt,[†] and Manuel Gruber*,[¶]

[†]*Institut für Experimentelle und Angewandte Physik, Christian-Albrechts-Universität zu Kiel, 24098 Kiel, Germany*

[‡]*LCC, CNRS and Université de Toulouse, UPS, INP, 31077 Toulouse, France*

[¶]*Faculty of Physics and CENIDE, University of Duisburg-Essen, 47057 Duisburg, Germany*

E-mail: manuel.gruber@uni-due.de

1 Molecule removal from an island

Figure S1 shows a series of images illustrating the sequential removal of single molecules from an island. For picking up a molecule, the tip is positioned above the targeted molecule and the tunneling parameters are adjusted to 50 mV and 5 pA. The current feedback remained active during the entire procedure. The tip is then approached toward the molecule by increasing the current to 20 pA. After typically 50 ms, the current increased to $\approx$ 65 pA and the feedback responded by retracting the tip by $\approx$ 180 pm. The tip was then indented in the Cu(111) substrate to remove the attached molecule from the tip. As discussed in the main text, the orientation of the depressions left behind indicates the orientation of the molecules within the layers. We removed up to 6 molecules from a single island. All resulting depressions exhibit the same orientation. In particular, we verified that molecules belonging to adjacent rows and columns have the same orientation.

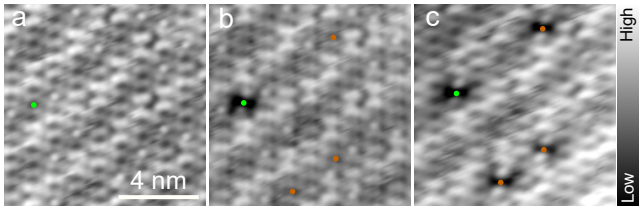

Figure S1: **a**–**c** Series of constant-current topographs of $[Fe(HB(1,2,4\text{-triazol-1-yl})_3)_2]$ on Cu(111) (200 mV, 5 pA, $10\times10\,nm^2$) illustrating the evolution of a layer as single molecules are removed. The procedure described in the text was applied to the molecule marked with a green dot in **a**, which leads to a depression in the molecular layer after the manipulation (shown in **b**). The molecule removal procedure was then repeated on the molecules marked with an orange dot, leading to the image shown in **c**. The color scales cover **a** 105 pm and **b**–**c** 100 pm.

2 Adsorption-induced chirality

We assume that the molecules lie flat on the surface with the B-Fe-B axis parallel to the surface. A triazole group from each of the two scorpionate ligands makes the contact to the surface (see for instance Figure S2a). Viewed along the B-Fe-B axis, the angle between the triazole groups in contact with the substrate is approximately 60°. The configuration shown in Figure S2b is obtained by rotating the molecule by −60° around the B-Fe-B axis. An azimuthal rotation of the molecule displayed in Figure S2a around the axis perpendicular to the surface cannot lead to that in Figure S2b (see also top views in Figures S2c–d). In other words, the adsorption of the molecule on the surface induces a chirality.

The depression left behind upon the removal of a molecule provides information on the orientation of the molecule defined by the upper triazole groups (opaque atoms in Figures S2c–d), which is the same for all molecules within an island. The periodicity of the molecular structure is directly inferred from the STM images. Attempts to reproduce the regular structure observed in Figure 2 of the manuscript by using the enantiomer shown in Figure S2b, and with a combination of both enantiomers failed due to unphysical partial overlap of the molecules. Only the structure composed of solely the enantiomer shown in Figures S2a,c led to a reasonable result, the one displayed in Figure 2 of the manuscript.

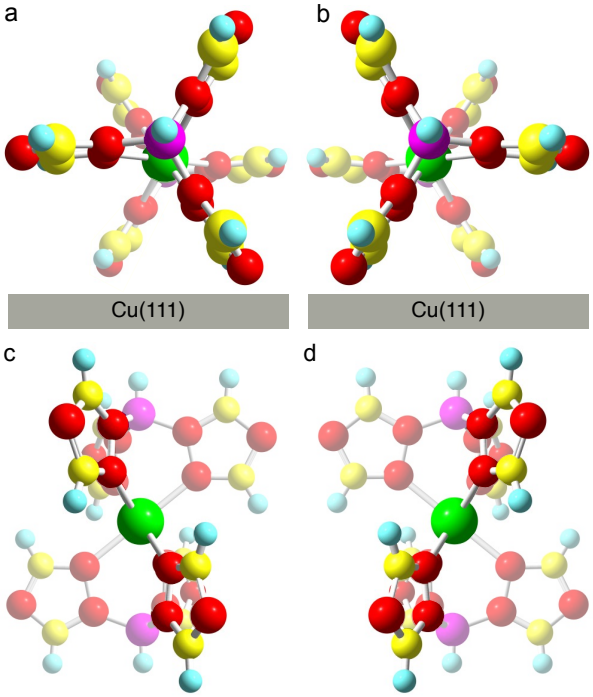

Figure S2: **a**–**b** View of the [Fe(HB(1,2,4-triazol-1-yl)$_3$)$_2$] molecule along the B-Fe-B axis adsorbed on a Cu(111) surface. From **a** to **b** the molecule is effectively rotated by −60° around the B-Fe-B axis. The two configurations correspond to two adsorption-induced enantiomers. **c**–**d** Corresponding top views of the configurations. The transparency of the atoms indicates the distance from the observer. Opaque atoms are closer than semi-transparent atoms.

3 Chirality of islands

As the chirality is induced by adsorption, both enantiomers are expected to be present on the surface. If an island is indeed composed of a single enantiomer, different islands will be present on the surface. This is indeed the case. As detailed in the main text, the islands exhibit stripes, which make them chiral. For instance, the island of Figure S3a has stripes going from the top left to the bottom right. Azimuthal rotation of that island cannot reproduce the island shown in Figure S3b. The removal of molecules from these islands reveals different orientations of the depressions (Figures S3c–d), and hence different orientations of the molecules.

The island shown in Figure S3a is equivalent to that shown in Figure 2 of the manuscript, with the molecular structure shown in Figure S3g. Attempts to reproduce the island shown in Figure S3b using the same enantiomer failed due to unphysical overlaps. Instead, the structure shown in Figure S2h made with the other enantiomer leads to a good match. The two structures are equivalent in terms of the molecule-molecule interactions but are chiral.

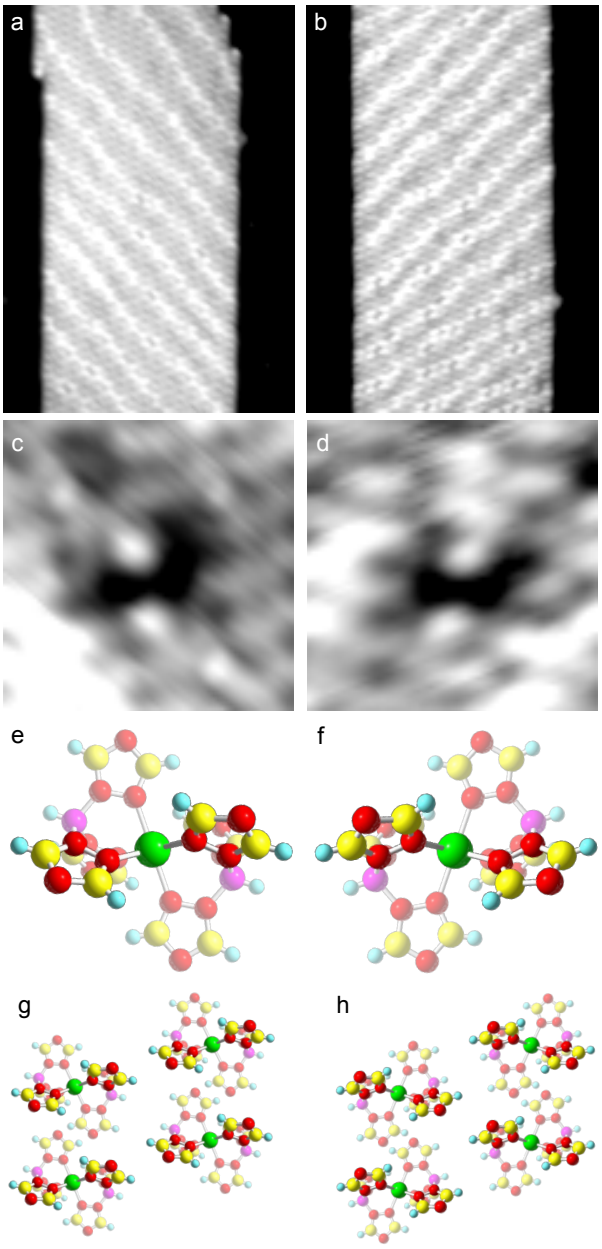

Figure S3: **a**–**b** STM images displaying the chirality of the islands. The island in **a** exhibits stripes from the top left to the bottom right. An azimuthal rotation of **a** cannot reproduce the pattern in **b**, which was observed on the same sample. **c** and **d** Depressions after removal of a molecule from the islands in **a** and **b**, respectively. The molecular structures of island **a** and **b** may be reproduced by using the enantiomers **e** and **f**, respectively. The corresponding molecular structures are shown in **g** and **h**.

4 Reduced height of edge molecules

Molecules at the edge of an island appear $\approx 55\,\mathrm{pm}$ lower than molecules within islands at 1.6 V (see for instance the left column in the inset of Figure S4). Red circles in Figure S4 shows a cross-sectional profile of an island edge. The height difference may be understood from a simple model that takes into account the lateral extension of the tip. The limited lateral resolution implies that the current above the center of a molecule is increased by the contributions of the neighbors, which are fewer for a molecule at an edge. Adding these current contributions with exponentially decaying weight the experimental data may be qualitatively reproduced (black curve in Figure S4).

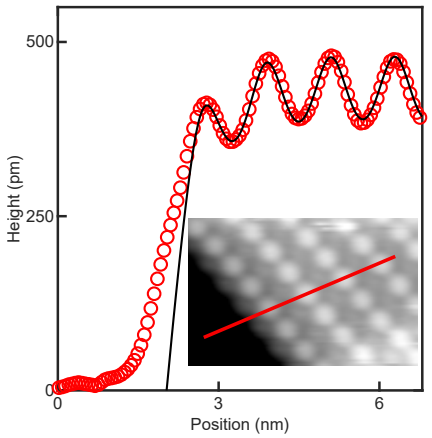

Figure S4: Cross-sectional profile of a [Fe(HB(1,2,4-triazol-1-yl)$_3$)$_2$] island edges along the line shown in the topograph in the inset ($V = 1.6\,\mathrm{V}$, $I = 5\,\mathrm{pA}$). Red circles show experimental data. The black line results from a simple model of a tip with limited lateral resolution. No attempt was made to fit the data at low apparent heights because the large vertical excursion of the tip of the STM implies that the unknown three-dimensional tip structure must be taken into account.